IRIS AperTO

UNIVERSITÀ DEGLI STUDI DI TORINO

AperTO - Archivio Istituzionale Open Access dell'Università di Torino

Remote sensing of larch phenological cycle and analysis of relationships with climate in the Alpine region

This is the author's manuscript

Original Citation:

Availability:

This version is available http://hdl.handle.net/2318/100317 since 2016-09-08T17:40:05Z

Published version:

DOI:10.1111/j.1365-2486.2010.02189.x

Terms of use:

Open Access

Anyone can freely access the full text of works made available as "Open Access". Works made available under a Creative Commons license can be used according to the terms and conditions of said license. Use of all other works requires consent of the right holder (author or publisher) if not exempted from copyright protection by the applicable law.

(Article begins on next page)

27 November 2024

IRIS AperTO

UNIVERSITÀ DEGLI STUDI DI TORINO

This is the author's final version of the contribution published as:

L. Busetto; R. Colombo; M. Migliavacca; E. Cremonese; M. Meroni; M. Galvagno; M. Rossini; C. Siniscalco; U. Morra di Cella; E. Pari. Remote sensing of larch phenological cycle and analysis of relationships with climate in the Alpine region. GLOBAL CHANGE BIOLOGY. 16(9) pp: 2504-2517. DOI: 10.1111/j.1365-2486.2010.02189.x

The publisher's version is available at:
http://doi.wiley.com/10.1111/j.1365-2486.2010.02189.x

When citing, please refer to the published version.

Link to this full text:
http://hdl.handle.net/2318/100317

This full text was downloaded from iris - AperTO: https://iris.unito.it/

iris - AperTO

University of Turin's Institutional Research Information System and Open Access Institutional Repository

Remote sensing of larch phenological cycle and analysis of relationships with climate in the Alpine region

Authors

L. Busetto; R. Colombo; M. Migliavacca; E. Cremonese; M. Meroni; M. Galvagno; M. Rossini; C. Siniscalco; U. Morra di Cella; E. Pari

- First published: 22 January 2010Full publication history
- DOI: 10.1111/j.1365-2486.2010.02189.xView/save citation
- Cited by: 5 articles

L. Busetto, Laboratorio di Telerilevamento delle Dinamiche Ambientali, Dipartimento di Scienze dell'Ambiente e del Territorio, Università di Milano-Bicocca, Piazza della Scienza 1, 20126 Milano, Italy, tel. +39 02 64482819, fax +39 02 64482895, e-mail: lorenzo.busetto@unimib.it

Abstract

This research aims at developing a remote sensing technique for monitoring the interannual variability of the European larch phenological cycle in the Alpine region of Aosta Valley (Northern Italy) and to evaluate its relationships with climatic factors. Phenological field observations were conducted in eight test sites from 2005 to 2007 to determine the dates of completion of different phenological phases. MODerate Resolution Imaging Spectrometer (MODIS) 250 m 16-days normalized difference vegetation index (NDVI) time series were fitted with double logistic curves and the dates corresponding to different features of the curves were determined. Comparison with field data showed that the features of the fitted NDVI curve that allowed the best estimate of the start and end of the growing season were the zeroes of its third derivative (MAE of 6 and 4 days, respectively). The start and end of season were also estimated with the spring warming (SW) and growing season index (GSI) phenological models. MODIS start and end of season dates generally agreed with those obtained by the SW and GSI climate-driven phenological models. However, phenological models provided erroneous results when applied in years with anomalous meteorological conditions. The relationships between interannual variability of the larch phenological cycle and climate were investigated by comparing the mean start and end of season yearly anomalies with air temperature anomalies. A strong linear relationship (R^2=0.91) was found between mean spring temperatures and mean start of season dates, with an increase of 1 °C in mean spring temperature leading to a 7-day anticipation of mean larch bud-burst date. Leaf coloring dates were found to be best related with mean September temperature (R^2=0.77), but with higher spring temperatures appearing to lead to earlier leaf coloring.

Nomenclature:
$A_{1..5}$=NDVI metrics computed in the Autumn season
$AP_{1..5}$=Autumn phenological phases
DOY=Day of the year
EF=Modeling efficiency
EOS_{GSI}=End of season date estimated by the GSI model
EOS_{MODIS}=End of season date estimated from MODIS data

ΔEOS_{MODIS} = Yearly anomaly of MODIS end of season of one pixel with respect to its 2000–2007 mean
$\overline{\Delta EOS_{MODIS}}$ = Mean regional yearly anomaly of MODIS end of season
EOS_{OBS}=End of season date estimated from field observations
GSI=Growing season index
GSL=Growing season length
MAE=Mean absolute error
ME=Mean error
MODIS=MODerate Resolution Imaging Spectrometer
NDVI=Normalized difference vegetation index
r = Pearson's correlation coefficient
R^2_{adj}= Adjusted coefficient of determination of the multiple regression
$S_{1..5}$=NDVI metrics computed in the spring season
SOS_{GSI}=Start of season date estimated by the GSI model
SOS_{MODIS}=Start of season date estimated from MODIS data
ΔSOS_{MODIS}= Yearly anomaly of MODIS start of season of one pixel with respect to its 2000–2007 mean
$\overline{\Delta SOS_{MODIS}}$ = Mean regional yearly anomaly of MODIS start of season
SOS_{OBS}=Start of season date estimated from field observations
SOS_{SW}=Start of season date estimated by the SW model
$SP_{1..5}$=Spring phenological phases
SW=Spring warming
VI=Vegetation indexes

Introduction

Phenology is the study of recurrent biological events and the causes of their temporal change due to biotic and abiotic forces (Lieth, 1974). As regards plants, phenological studies provide an understanding of the timing of the main seasonal events, such as bud-burst, flowering, leaf coloring or leaf fall. Since this timing is a consequence of the relationships between vegetation and climatic and other ecological drivers (e.g., air temperature, photoperiod, snow cover, soil moisture), the analysis of its variations can be exploited to evaluate the effect of recent climatic change on terrestrial ecosystems (e.g., Chen *et al.*, 2000; Chuine, 2000; Kramer *et al.*, 2000; White *et al.*, 2003; Badeck *et al.*, 2004). The study of plant phenology and its relationships with climate is particularly important in Alpine regions, since these areas are considered to be highly sensitive to climate change (e.g., Beniston & Rebetez, 1996; Theurillat & Guisan, 2001).

Several studies based on analysis of time series of field phenological observations have shown evidence of an overall increase in growing season length (GSL) in the mid and high latitudes of the northern hemisphere in the last decades, generally related to an increase in air temperature (e.g., Menzel & Fabian, 1999; Rötzer *et al.*, 2000; Schwartz & Reiter, 2000; Cayan *et al.*, 2001; Defila & Clot, 2001; Chmielewski & Rötzer, 2002; Matsumoto *et al.*, 2003; Schaber & Badeck, 2005; Studer *et al.*, 2005).

Local field observations are work-intensive and difficult to extrapolate to large areas. For this reason, multitemporal coarse resolution satellite images (1–8 km pixel size) have been extensively used to map the timing of phenological events at regional or continental scales, also providing evidence of an increase in GSL in boreal areas in the last decades, mainly related to an earlier start

of the growing season (Myneni *et al.*, 1997; Zhou *et al.*, 2001; Bogaert *et al.*, 2002; Slayback *et al.*, 2003; Stöckli & Vidale, 2004).

Satellite phenological monitoring is usually based on the analysis of time series of spectral vegetation indexes (VI) derived from multispectral images. The timing of phenological events is estimated by identifying the dates corresponding to particular features (so-called VI metrics) of the annual VI time series. Several different metrics, such as fixed or local thresholds (White *et al.*, 1997; Studer *et al.*, 2007), points of maximum slope of the time series (e.g., Schwartz *et al.*, 2002; Cook *et al.*, 2005) or inflection points of mathematical curves fitted to the VI curves (Zhang *et al.*, 2003; Beck *et al.*, 2006; Fisher *et al.*, 2006) have been proposed in the literature. Since the use of different metrics can provide very different results (White *et al.*, 2009), a detailed comparison between satellite estimates and field-observed dates of phenological events is needed in order to identify an objective criterion for estimating, for example, the dates of the start and end of the growing season from satellite data (Reed *et al.*, 1994; Schwartz & Reed, 1999). Such comparisons have however been seldom performed in the literature (e.g., Delbart *et al.*, 2005, 2006; Beck *et al.*, 2007; Fisher & Mustard, 2007; Soudani *et al.*, 2008) and provided contrasting results, also because of the large scale difference between coarse resolution satellite data and local phenological field observations (Fisher & Mustard, 2007). Only recently, MODIS images with pixel size of 250 m have been available for phenological mapping at higher spatial resolution, thus facilitating comparison between satellite estimates and field data (e.g., Ahl *et al.*, 2006; Beck *et al.*, 2006, 2007; Soudani *et al.*, 2008).

Besides field observations and satellite data, climate-driven phenological models are also an important tool for understanding phenological responses to interannual climatic variability, offering a unique opportunity to analyze the roles of the different factors governing plant phenology. For boreal and alpine species, phenological models taking into account only the action of air temperature as a driver of plant spring development are often used for the prediction of start of season dates (Hunter & Lechowicz, 1992; Picard *et al.*, 2005). Simulation of end of season and GSL is instead less common (Jolly *et al.*, 2005; Richardson *et al.*, 2006; Delpierre *et al.*, 2009), since the role of the different factors influencing senescence has not yet been clearly understood (Worrall, 1999; Schaber & Badeck, 2002). The comparison between satellite estimates and phenological models can provide useful information both to understand the relationships between the satellite signal and plant phenological development, and to analyze the accuracy of climate-driven models on large areas (Fisher *et al.*, 2007). This comparison has seldom been made in the literature, showing moderate to good agreement between results obtained with the two methods (e.g., Schwartz *et al.*, 2002; Fisher *et al.*, 2007; Delbart *et al.*, 2008).

In this paper, we present a study aimed at analyzing the interannual variability of the European larch phenological cycle in a mountainous Alpine area by using a combination of field observations, satellite data and phenological models. To this end, the performances of several VI metrics extracted from MODIS 250 m images for monitoring different phases of the larch phenological cycle were evaluated through comparison with field data collected in different years. The accuracy of the start and end of season dates estimated from MODIS was assessed and compared with that of two climate-driven phenological models. Regional start and end of season maps derived from MODIS data were finally analyzed to identify the relationships between larch phenology and air temperatures. This allowed a simple quantification of the response of European larch to interannual climatic variability in a sensitive terrestrial environment such as the Alps.

Materials and methods

Study area and phenological field observations

The study was conducted on European larch (*Larix decidua* Mill.) forests in the Aosta Valley (Northwestern Italy), a typical Alpine region with considerable variations in elevation and terrain morphology (Fig. 1).

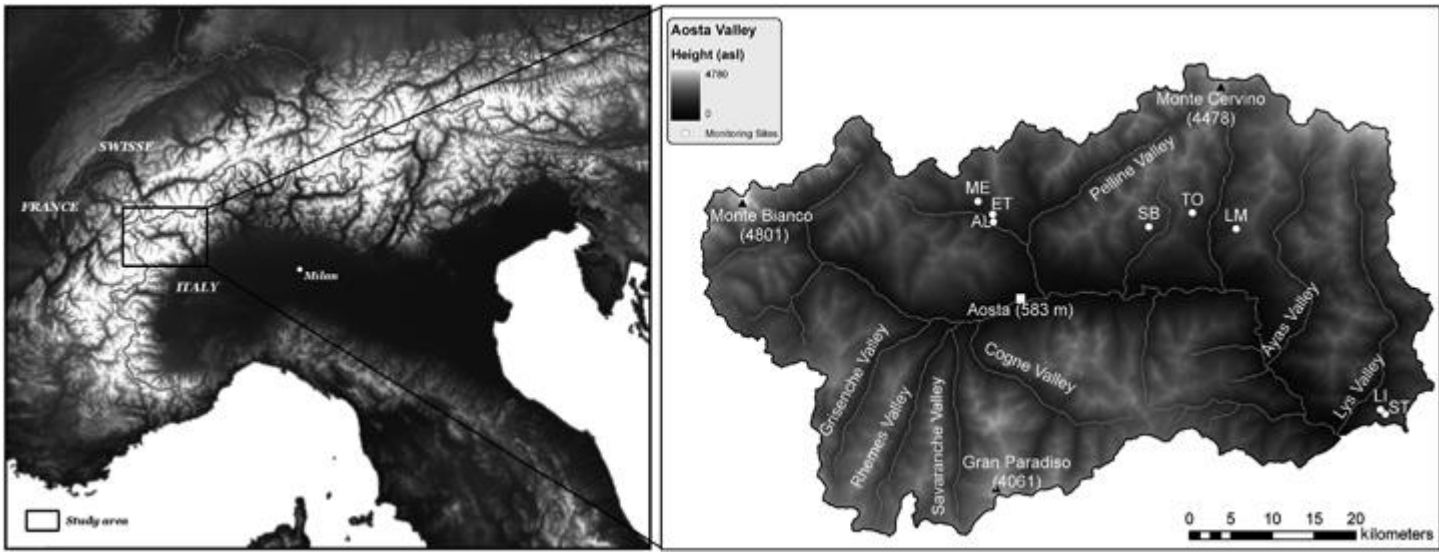

Figure 1. Location of the study area and the eight monitoring sites.

The European larch is a conifer widely distributed in the Alps which is well suited for phenological studies based on satellite data. Differently from the other conifers growing at high altitudes in the region, European larch is in fact a deciduous species, so that its phenological phases are more easily detectable from both field observations and remotely sensed data. Eight pure and homogeneous European larch communities were selected within the Aosta Valley. The eight sites cover a wide altitudinal range (1320–2160 m) and their spatial distribution encompasses the main climatic conditions of the region. Morphological parameters vary considerably from site to site. Mean slopes range between 14° and 52°, while exposures vary from E (110°) to NW (300°). No sites were selected in the N and NE quadrants to avoid shadowing problems on the satellite signal in the spring season. Basal area varies between 24.2 and 41.7 m^2 ha^{-1} and fractional cover of tree crowns is generally above 70%, with the exception of the Stouba site that showed a mean fractional cover of 44%. An extensive description of site characteristics can be found in Migliavacca *et al.* (2008).

Three sampling plots located at different heights were identified in each site. Field observations were conducted in each plot in spring and autumn of 2005, 2006 and 2007 with a frequency of about 1 week to identify the dates of completion of the 10 phenological phases described in Fig. 2. Observations were conducted in all eight sites during 2005, while in 2006 and 2007 three of them were excluded because of logistical constraints.

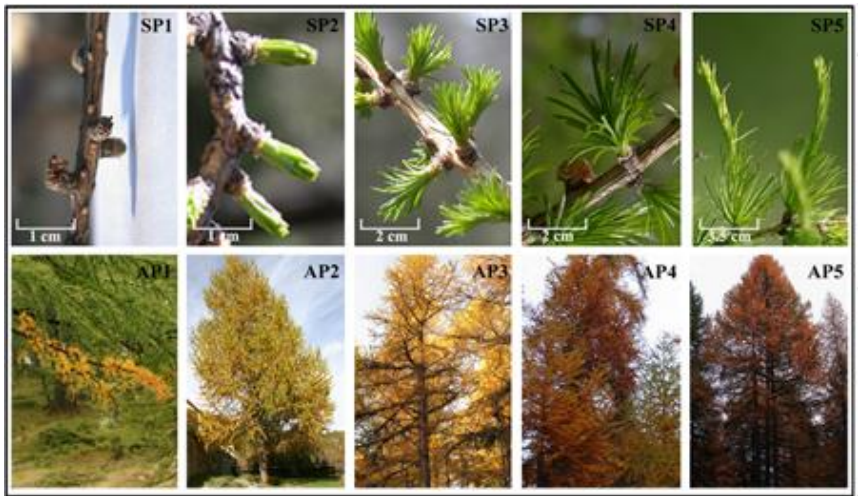

Phenological Phase	Score	Description
SP_1	1	Winter Conditions, unexpanded buds (LAI Overstory = 0)
SP_2	2	Bud-burst. Needles Length < 1 cm (Start of season)
SP_3	3	Needles Elongation. Length 1–3 cm
SP_4	4	Needles Elongation. Length > 3 cm
SP_5	5	Needles Fully Exponded (Maximum LAI)
AP_1	1	Yellow spot coloration
AP_2	2	Green to yellow phase
AP_3	3	Complete crown yellowing (End of season)
AP_4	4	Yellow to red phase
AP_5	5	Complete crown reddening

Figure 2. Visual representation and description of the spring (SP) and autumn (AP) phenological phases identified in the field surveys.

During springtime, phase SP_2 corresponds to bud-burst while the other phases are identified on the basis of needle elongation. Autumn senescence phases are instead identified on the basis of leaf coloring. For example, phase AP_1 corresponds to the appearance of yellowing spots at the apical portion of basal and medial branches while phase AP_3 is reached when yellowing occurs on the whole tree crown.

At each field survey, a score ranging from 1 to 5 was assigned to 10 trees randomly selected near the center of each plot, as a function of the achieved phenological phase. Subjectivity in the assignment of phenological scores was reduced as much as possible by limiting the number of operators and performing preliminary training sessions. The dates of completion of each phenophase at plot level were then computed by linearly interpolating the average score of its 10 trees against the sampling dates and determining the date at which the interpolated value reached the score corresponding to each phase (Migliavacca *et al.*, 2008). This computation scheme leads to uncertainties in the estimated dates smaller than the time interval between the two field campaigns conducted before and after the computed completion date, minus 1 day.

The completion dates at site level were finally computed as the mean of the dates of its three plots. The start of season at site level (SOS_{OBS}) was defined to coincide with the date of completion of phase SP_2, while the end of season (EOS_{OBS}) was defined to coincide with the date of completion of phase AP_3. In the spring season an additional phase was computed to verify the possibility of detecting the earliest spring phenological phases from satellite data ($SP_{1.5}$: bud-burst completed on 50% of the trees).

Computation of remote sensing metrics

MODIS normalized difference vegetation index (NDVI) preprocessing. All the 184 MODIS TERRA 16-day composite NDVI images with 250 m spatial resolution (MOD13Q1 Product – v005) acquired in the period 2000–2007 were downloaded from the EOS Data Gateway distributed archive.[1] MOD13Q1 NDVI values are computed by applying the Constrained View Angle Maximum Value Composite algorithm on daily reflectance data acquired in the 16-day compositing period (Huete *et al.*, 2002). Auxiliary information regarding data quality and snow cover conditions at the time of acquisition are also provided on a per-pixel basis. Starting from collection v005, the Julian day of acquisition of data used to compute the composite NDVI is also provided. This is of

great importance for phenological monitoring from satellite data, since it allows association of the composite NDVI values with their true acquisition dates.

MODIS images were re-projected from the native SIN projection to a UTM-WGS84 reference system and resized on the study area using the 'modis reprojection tool v. 4.0' software.[2] MODIS images acquired at different times were assumed to be well co-registered, so that no further geometric correction was performed. The effect of noise caused by cloud contamination, atmospheric variability and bi-directional effects, which can compromise the possibility of monitoring the vegetation phenological cycle from NDVI data (Sakamoto *et al.*, 2005), was reduced by applying the smoothing procedure proposed in Chen *et al.* (2004).

Winter NDVI values of larch forests in the Aosta Valley are typically negatively biased by the effect of snow cover. This makes it difficult to distinguish the NDVI increase due to vegetation growth from that due to snow melting (Delbart *et al.*, 2005; Studer *et al.*, 2007). In order to overcome this problem, a winter NDVI value ($NDVI_w$) was computed for each larch forest pixel and assumed to represent the typical NDVI that would have been observed in absence of snow during the larch dormancy phase, as suggested in Beck *et al.* (2006, 2007). To this end, the NDVI values >0.3 recorded in snow-free conditions (according to the MODIS Snow Cover Flag) in the autumn and early winter of each year were extracted. The $NDVI_w$ of each larch pixel was then computed as the mean of the minimum values extracted in each year. NDVI values lower than $NDVI_w$ were finally replaced with $NDVI_w$, resulting in time series characterized by a constant value in the winter period.

Curve fitting and determination of NDVI metrics. A double logistic function was fitted on the smoothed and snow-corrected MODIS time series to produce continuous NDVI curves. The double logistic was demonstrated to be particularly well suited for phenological monitoring from remote sensing data (Beck *et al.*, 2006; Fisher *et al.*, 2006). This function allows asymmetry in the NDVI temporal evolution of spring and autumn but assumes an equal but opposite curvature at the start and end of the leaf unfolding (or leaf coloring) seasons, which may lead to a reduction of its ability to fit the NDVI time series (Beck *et al.*, 2006).

The double logistic function describes the NDVI time series as follows:

$$\mathrm{NDVI}(i,t) = \mathrm{NDVI}_w(i) + (\mathrm{NDVI}_{MAX}(i) - \mathrm{NDVI}_w(i)) \left(\frac{1}{1+e^{-mS\cdot(t-S)}} + \frac{1}{1+e^{mA\cdot(t-A)}} - 1\right), \quad (1)$$

where $(\mathrm{NDVI}(i,t))$ is the NDVI of pixel *i* at day of the year (DOY) *t*, $\mathrm{NDVI}_{MAX}(i)$ is the maximum NDVI during the year, *S* and *A* are the DOYs of maximum slope of the curve, respectively, in spring and autumn, whereas *mS* and *mA* are the slopes of the curve at DOYs *S* and *A*.

For each pixel and year, the five parameters describing the shape of the fitting curve were determined by least squares minimization of the differences between Eqn (1) and the MODIS NDVI time series. This was accomplished through the use of a Levenberg–Marquardt curve-fitting algorithm (MPFIT –Markwardt, 2008). The DOYs at which the fitted logistic curves showed characteristic curvature changes (NDVI metrics) were then identified with the equations shown in Table 1.

Table 1. Equations used for the computation of NDVI metrics

Spring season (DOY)	Autumn season (DOY)
$S_1 = \frac{2\ln(\sqrt{3}-\sqrt{2})}{mS} + S$	$A_1 = \frac{2\ln(\sqrt{3}-\sqrt{2})}{mA} + A$
$S_2 = \frac{\ln(2-\sqrt{3})}{mS} + S$	$A_2 = \frac{\ln(2-\sqrt{3})}{mA} + A$
$S_3 = S$	$A_3 = A$
$S_4 = \frac{\ln(2+\sqrt{3})}{mS} + S$	$A_4 = \frac{\ln(2+\sqrt{3})}{mA} + A$
$S_5 = \frac{2\ln(\sqrt{3}+\sqrt{2})}{mS} + S$	$A_5 = \frac{2\ln(\sqrt{3}+\sqrt{2})}{mA} + A$

1. *mS* and *mA* are the values of maximum slope of the fitting curve in spring and autumn, occurring, respectively, at DOY *S* and *A*.

Five metrics were identified in both the spring and autumn seasons. Metrics S_3 and A_3 are the dates of maximum increase (decrease) of the fitted curve, which also correspond to the dates at which the curve reaches its half-maximum value. These metrics are frequently used to estimate the start and end of season dates from remote sensing data (e.g., White *et al.*, 1997; Badeck *et al.*, 2004; Fisher & Mustard, 2007). Metrics S_2,S_4 and A_2,A_4 are the dates of transition between the linear and nonlinear portions of the sigmoid curve (Potts *et al.*, 1993), and correspond to the roots of the third derivative of the fitted curve. Metrics S_1,S_5 and A_1,A_5 are the dates at which the rate of change in curvature in the NDVI data exhibits local minima or maxima, and correspond to local maxima and minima of the third derivative of the fitted curve. These metrics were previously used to estimate the dates of start and end of season, onset of maximum leaf area and dormancy (Ahl *et al.*, 2006).

Results of curve-fitting and NDVI metrics estimation for one of the pixels corresponding to the Torgnon site is shown as an example in Fig. 3.

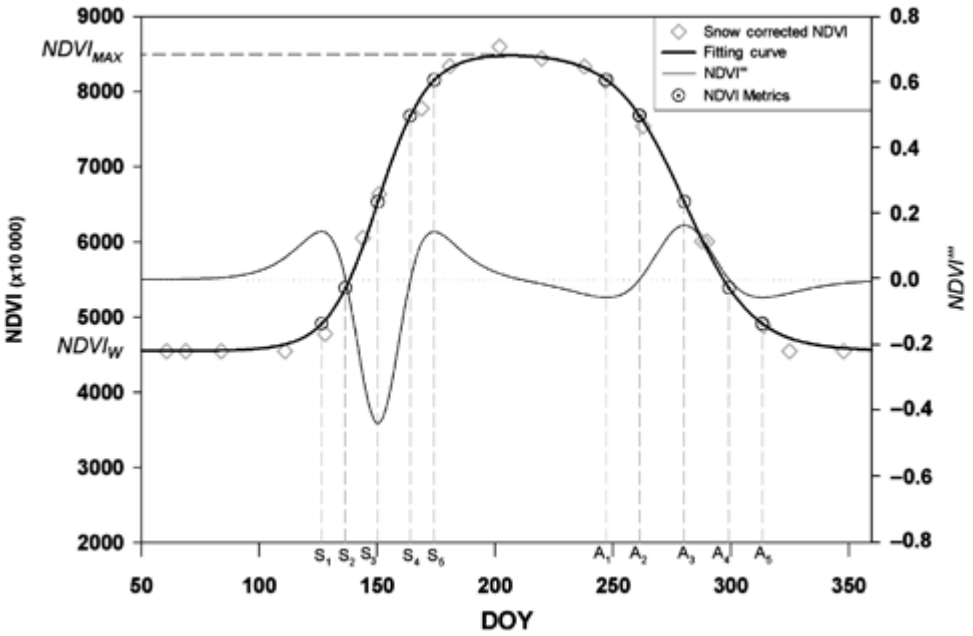

Figure 3. Results of the double logistic curve fitting on MODIS NDVI of one pixel of the Torgnon site (year 2003) and position of the different NDVI metrics on the fitted curve and on its third derivative.

Computation of start and end of season from phenological models

The start and end of season of larch at five of the monitoring sites were also estimated using the spring warming (SW –Chuine, 2000; Picard *et al.*, 2005) and the growing season index (GSI –Jolly *et al.*, 2005) phenological models, to provide an intercomparison of results achieved with satellite estimates and climate-driven models.

The two models were selected because their input parameters had been optimized for application to European larch forests of the Aosta Valley in a recent study (Migliavacca *et al.*, 2008). SW allows estimation only of start of season dates and assumes that from a specific day of the year (usually the 1st of January) plants accumulate 'heat units' when mean daily air temperature exceeds a specified base temperature. Start of season (SOS_{SW}) is assumed to occur when a critical sum of heat units (F^*) is reached. GSI allows estimation of both start and end of season dates. The meteorological drivers of the model are daily minimum temperature, vapor pressure deficit (VPD) and photoperiod. Start of season (SOS_{GSI}) is assumed to occur when the moving average with 21 days width of a daily index computed from meteorological inputs exceeds a user-defined threshold in spring, while end of season (EOS_{GSI}) is assumed to occur when the moving average drops below the same threshold in autumn.

In order to apply the models, mean and minimum daily air temperatures were derived from hourly data measured by weather stations installed in the central phenological monitoring plot of the five sites in 2005. Daily diurnal VPD was estimated from mean diurnal and minimum daily temperatures (the latter assumed to be equal to the dewpoint temperature) as suggested by Campbell & Norman (1998). Finally, the daily photoperiod of each site was computed using incoming radiation simulated with the Solar Analyst model (Fu & Rich, 1999).

Comparison of field observations with NDVI metrics and phenological models estimates

The field monitoring sites were accurately identified on MODIS images with the aid of detailed orthophotos. The dimension of the different sites varied from four to seven MODIS pixels, and the coefficient of variation of the NDVI signal during the larch growing season was generally lower than 10%. NDVI metrics for each site were computed as the mean of results obtained in its different pixels.

The performance of the different NDVI metrics for monitoring the different larch phenophases was then evaluated by computing the correlation coefficient (r), the mean estimation error (ME) and its standard deviation, the mean absolute error (MAE) and the modeling efficiency (EF –Nash & Sutcliffe, 1970) between results obtained with each metric at the monitoring sites and the in-field observed dates of completion of each phenological phase. ME quantifies the tendency of the selected metric to overestimate or underestimate the DOY of completion of the selected phenophase, while MAE measures the expected difference (expressed in number of days) between the NDVI metric and the completion DOY. Finally, EF is a synthetic indicator of the efficiency of the metric in predicting the completion DOY, sensitive to systematic deviations between observed and estimated data (Janssen & Heuberger, 1995). The combined analysis of these different statistical parameters provides a thorough understanding of the accuracy of the estimates. In particular, good accuracy of one metric for estimation of one of the phenophases dates is evidenced by the combination of a high r, a near-zero ME, a low MAE and an EF near one.

The metrics showing the best performances for estimating phenophases SP_2 and AP_3 (which correspond to SOS_{OBS} and EOS_{OBS}) were identified and successively used to compute the start and end of season of larch forests in the entire Aosta Valley from MODIS data (SOS_{MODIS}, EOS_{MODIS}).

The accuracy of the SW and GSI models for estimating the field-observed start and end of season dates was evaluated using the same statistical indicators and compared with that of MODIS estimates. The comparison was conducted considering only results obtained in 2006 and 2007 because phenological models were parameterized by inversion against 2005 field data, so that the inclusion of 2005 data in the analysis would have resulted in an overestimation of the accuracy of phenological models (Migliavacca *et al.*, 2008).

Comparison between phenological and climatic interannual variations at regional level

Larch forests of the Aosta Valley were identified on MODIS images on the basis of a map derived from visual interpretation of aerial ortophotos. Regional maps of SOS_{MODIS} and EOS_{MODIS} for the 2000–2007 time period were then computed using the best performing NDVI metrics, identified as described in the above section. GSL_{MODIS} was then computed as the difference between SOS_{MODIS} and EOS_{MODIS}. For each pixel, the yearly anomalies of SOS_{MODIS} and EOS_{MODIS} with respect to its 2000–2007 mean were also determined (ΔSOS_{MODIS}, ΔEOS_{MODIS}). The mean yearly regional anomalies ($\overline{\Delta SOS}_{MODIS}$, $\overline{\Delta EOS}_{MODIS}$) were finally computed to provide an indication of the mean interannual variability of the larch phenological cycle. To avoid errors due to the presence of different land cover types in the MODIS footprint this analysis was performed considering only pixels showing a fractional cover of larch >80%.

The relationships between interannual variability of the larch phenological cycle and regional climate were then investigated by comparing the satellite-derived phenological anomalies with yearly air temperature anomalies in different periods of the year. Daily mean temperatures measured at 10 automatic meteorological stations of the Aosta Valley meteorological service providing complete records from 2000 to 2007 were used for the analysis. The stations are located in different areas of the region and span an elevation range between 594 and 2050 m asl. For each station and year, the anomaly of mean monthly temperatures and of their running averages with periods of 2, 3 and 4 months (e.g., Mean temperature of February, March and May) with respect to the corresponding 2000–2007 mean were computed. Yearly regional temperature anomalies ($\overline{\Delta T}_m$, with *m* indicating the month or months considered) were then calculated as the mean of the anomalies observed at the 10 stations in the year considered.

$\overline{\Delta T}_m$ were then used as independent predictors in a stepwise multiple regression analysis exploiting $\overline{\Delta SOS}_{MODIS}$ and $\overline{\Delta EOS}_{MODIS}$ as the dependent variables. This allowed determination of the temperature anomalies best related to phenological anomalies in terms of R^2 adjusted (R^2_{adj}) of the multiple regression.

Results

Relationship between larch phenophases and NDVI metrics

Results of the statistical analysis conducted to assess the suitability of the different NDVI metrics for estimating the different phenophases dates are given in Table 2.

Table 2. Results of the statistical comparison between MODIS NDVI metrics and phenophases dates

NDVI metric	Phenological phase	*N*	*r* (**P*<0.001 *P*<0.01)	ME (± 1SD) (days)	MAE (days)	EF	NDVI metric	Phenological phase	*N*	*r* (**P*<0.001 *P*<0.01)	ME (± 1SD) (days)	MAE (days)	EF
S_1	**$SP_{1.5}$**	**18**	**0.84****	**−1.34 (± 8.57)**	**7.11**	**0.57**	A_1	AP_1	15	0.77**	−29.84 (± 7.15)	29.84	−23.39
	SP_2 (≡SOS_{OBS})	18	0.88**	−7.81 (± 7.51)	8.27	0.38		AP_2	15	0.81**	−35.57 (± 6.55)	35.57	−26.81
	SP_3	18	0.93**	−19.28 (± 5.94)	19.28	−1.26		AP_3 (≡EOS_{OBS})	15	0.81**	−40.56 (± 6.47)	40.56	−34.97
	SP_4	17	0.95**	−29.59 (± 5.68)	29.59	−4.27		AP_4	11	0.88**	−46.73 (± 5.42)	46.73	−41.60
	SP_5	14	0.86**	−42.39 (± 8.83)	42.39	−12.85		AP_5	11	0.69	−60.80 (± 11.6)	60.80	−15.55
S_2	$SP_{1.5}$	18	0.84**	7.44 (± 8.22)	8.49	0.28	A_2	AP_1	15	0.80**	−18.26 (± 5.90)	18.26	−8.51
	SP_2(≡SOS_{OBS})	**18**	**0.88****	**0.97 (± 7.31)**	**6.39**	**0.72**		AP_2	15	0.84**	−24.00 (± 5.25)	24.00	−11.81
	SP_3	18	0.93**	−10.50 (± 5.50)	10.50	0.23		AP_3 (≡EOS_{OBS})	15	0.85**	−28.98 (± 5.21)	28.98	−17.48
	SP_4	17	0.95**	−20.80 (± 5.68)	20.80	−1.66		AP_4	11	0.91**	−34.68 (± 4.23)	34.68	−22.49

1. For each combination of metric and phenological phase, *N* is the number of observations available, *r* the correlation coefficient between field-observed and MODIS-estimated dates (with *P* indicating the statistical significance of the correlation), ME(± 1SD) the mean and standard deviation of the estimation error, MAE the mean absolute error of the estimates and EF the Modelling Efficiency of the metric. Best results obtained with each metric (in terms of MAE) are shown in bold.

NDVI metric	Phenological phase	*N*	*r* (**P<0.001 *P<0.01)	ME (± 1SD) (days)	MAE (days)	EF
	SP_5	14	0.85**	−33.84 (± 8.84)	33.84	−7.98
	$SP_{1.5}$	18	0.83**	19.29 (± 8.08)	19.29	−1.63
	SP_2 (≡SOS_{OBS})	18	0.87**	12.83 (± 7.34)	13.05	−0.17
	SP_3	**18**	**0.93****	**1.36 (± 5.36)**	**4.26**	**0.84**
S_3	SP_4	17	0.94**	−8.93 (± 4.94)	8.93	0.40
	SP_5	14	0.84**	−22.32 (± 8.32)	22.32	−3.17
	$SP_{1.5}$	18	0.81**	31.11 (± 8.41)	31.11	−5.28
	SP_2 (≡SOS_{OBS})	18	0.84**	24.65 (± 7.90)	24.65	−2.60
	SP_3	18	0.91**	13.18 (± 5.85)	13.18	−0.15
S_4	**SP_4**	**17**	**0.93****	**2.89 (± 5.43)**	**4.91**	**0.79**
	SP_5	14	0.81**	−10.83 (± 8.62)	11.40	−0.38
	$SP_{1.5}$	18	0.79**	39.88 (± 8.80)	39.88	−9.10
	SP_2 (≡SOS_{OBS})	18	0.82**	33.42 (± 8.40)	33.42	−5.40
S_5	SP_3	18	0.89**	21.95 (± 6.44)	21.95	−1.90
A_5	AP_3 (≡EOS_{OBS})	15	0.70*	13.90 (± 5.90)	13.90	−3.82
	AP_5	11	0.73	−48.74 (± 11.1)	48.74	−9.78
	AP_1	**15**	**0.81****	**−2.61 (± 5.01)**	**4.42**	**0.21**
	AP_2	15	0.86**	−8.35 (± 4.36)	8.35	−0.86
A_3	AP_3 (≡EOS_{OBS})	15	0.85**	−13.33 (± 4.43)	13.33	−3.19
	AP_4	11	0.91**	−18.34 (± 3.57)	18.34	−5.71
	AP_5	11	0.77*	−32.40 (± 10.8)	32.40	−4.02
	AP_1	15	0.75*	12.99 (± 5.22)	12.99	−4.05
	AP_2	15	0.81**	7.26 (± 4.72)	7.26	−0.56
A_4	**AP_3(≡EOS_{OBS})**	**15**	**0.80****	**2.27 (± 4.85)**	**4.21**	**0.42**
	AP_4	**11**	**0.85****	**−2.12 (± 4.24)**	**3.72**	**0.60**
	AP_5	11	0.77*	−16.18 (± 11.1)	16.18	−0.61
	AP_1	15	0.67*	24.62 (± 6.09)	24.62	−15.67
	AP_2	15	0.72*	18.89 (± 5.74)	18.89	−7.25

NDVI metric	Phenological phase	*N*	*r* (**P<0.001 *P<0.01)	ME (± 1SD) (days)	MAE (days)	EF	NDVI metric	Phenological phase	*N*	*r* (**P<0.001 *P<0.01)	ME (± 1SD) (days)	MAE (days)	EF
	SP_4	17	0.91**	11.67 (± 6.03)	12.02	0.01		AP_4	11	0.76*	9.99 (± 5.43)	9.99	−1.44
	SP_5	**14**	**0.79****	**−2.29 (± 8.98)**	**7.41**	**0.41**		**AP_5**	**11**	**0.72**	**−4.07 (± 11.57)**	**7.77**	**0.40**

As regards the spring season, results show that the NDVI metric S_1 is reached before SOS_{OBS}, as shown by the negative ME with respect to phase SP_2 and by its higher accuracy in estimating phenophase $SP_{1.5}$. The start of season at site level can instead be accurately determined using metric S_2, as shown by the low ME (0.97 days), the relatively low MAE (6.39 days) and the high EF (0.72). This metric was therefore selected for regional mapping of the larch start of season. Metric S_3, although frequently used in the literature for the estimation of start of season dates, is reached 13 days after SOS_{OBS}. This metric instead allows estimation with good accuracy of phase SP_3, which is characterized by needle elongation up to 3 cm. Metric S_4 shows good agreement with phase SP_4, in which the needles are unfolded but not fully expanded, and thus precedes the onset of maximum leaf area, which is instead best predicted with the S_5 metric.

As regards autumn phenophases, the correlation coefficients, the EFs and the MAE between autumn NDVI metrics and field data are lower than those obtained in the spring season, mainly due to the lower variability of the senescence dates observed in the different test sites. NDVI metrics A_1 and A_2 strongly precede visible coloring of larch needles, as shown by the largely negative ME (−29.8 and −35.5 days, respectively) with respect to phenophase AP_1. The initial stage of needle coloring (yellow spot coloration−phenophase AP_1) corresponds to the half peak of the NDVI curve (metric A_3), while the complete yellowing of tree crowns (phenophase AP_3), which corresponds to EOS_{OBS}, can be best inferred using metric A_4 (ME=2.3, MAE=4.2). This metric was therefore selected for regional mapping of the larch end of season. However, metric A_4 shows its best performance in predicting phenological phase AP_4, which corresponds to the transition from yellow to red (ME=−2.1, MAE=3.7). Finally, metric A_5 is best related to the complete reddening of crowns, which occurs about 3 weeks after complete yellowing.

Comparison between MODIS and phenological models estimates

Figure 4 shows the comparison of SOS_{OBS} and EOS_{OBS} with the start and end of season dates estimated from MODIS and phenological models, for the years 2006 and 2007.

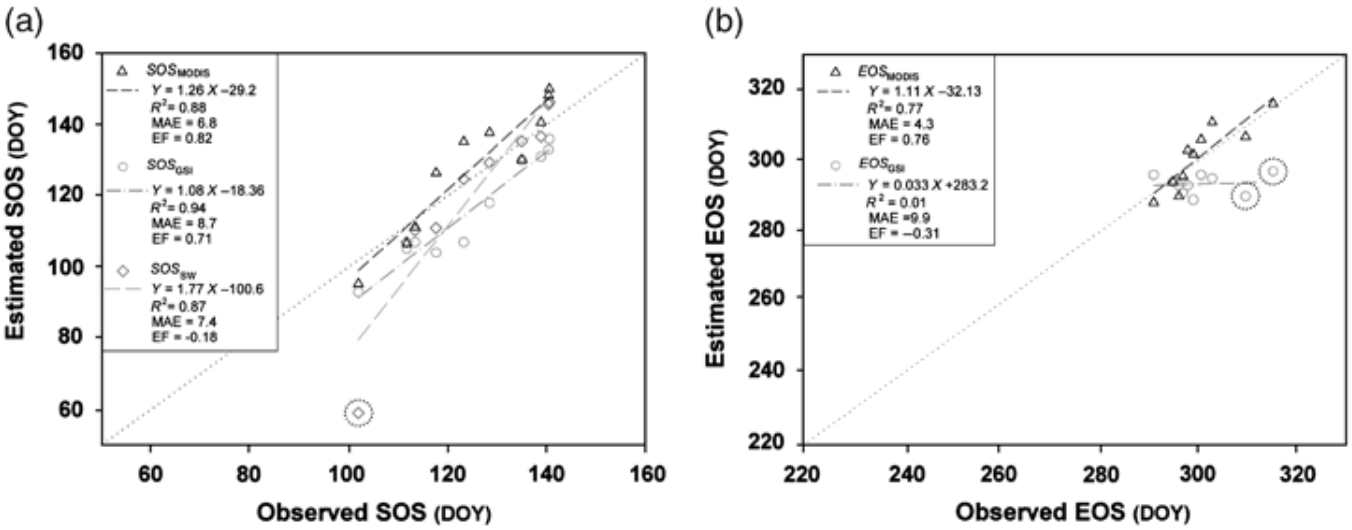

Figure 4. Comparison of start (a) and end (b) of season dates estimated from MODIS (SOS_{MODIS}, EOS_{MODIS}) and from the SW (SOS_{SW}) and GSI (SOS_{GSI}, EOS_{GSI}) models with field-observed dates (SOS_{OBS}, EOS_{OBS}). [Data highlighted by circles correspond to the 2007 SOS_{SW} (left panel) and the 2006 and 2007 EOS_{GSI} (right panel) estimates, at the Etroubles site.]

MODIS estimates of both start and end of season were more accurate than those obtained with phenological models, as shown by the lower MAE and higher EF values. SOS_{SW} provided a very accurate estimation of the start of season date in most of the sites, but in 2007 it produced an underestimation of 42 days at the Etroubles site, which caused a great reduction of the overall accuracy (MAE=9.3). Besides its very high correlation with SOS_{OBS}, SOS_{GSI} was found to underestimate the larch start of season, leading to a MAE of about 9 days. Contrary to what obtained with the SW model, the accuracy of SOS_{GSI} at the Etroubles site in 2007 was however similar to that of the other sites. GSI was also found to underestimate EOS_{OBS}, particularly at the Etroubles site, leading to a MAE of almost 10 days.

Spatial and interannual variability of start and end of season at regional level

Figure 5 shows, as an example, the regional maps of SOS_{MODIS}, EOS_{MODIS}, GSL_{MODIS} and of the corresponding anomalies with respect to the 2000–2007 mean, for the year 2003. The figure highlights the strong spatial variability of phenological dates across the study area, which is mainly related to altitudinal variations between the different larch stands and to their influence on air temperature (Migliavacca *et al.*, 2008; Colombo *et al.*, 2009). The effect of other primary topographic attributes (such as slope and aspect) on phenological development is instead difficult to ascertain, due to the confounding influence of cast shadows on radiation budget in morphologically complex areas. However, Colombo *et al.* (2009) recently showed that, at least at the higher elevations, the south-western and western slopes seem to show an advance in the start of the season with respect to the south-eastern and eastern ones.

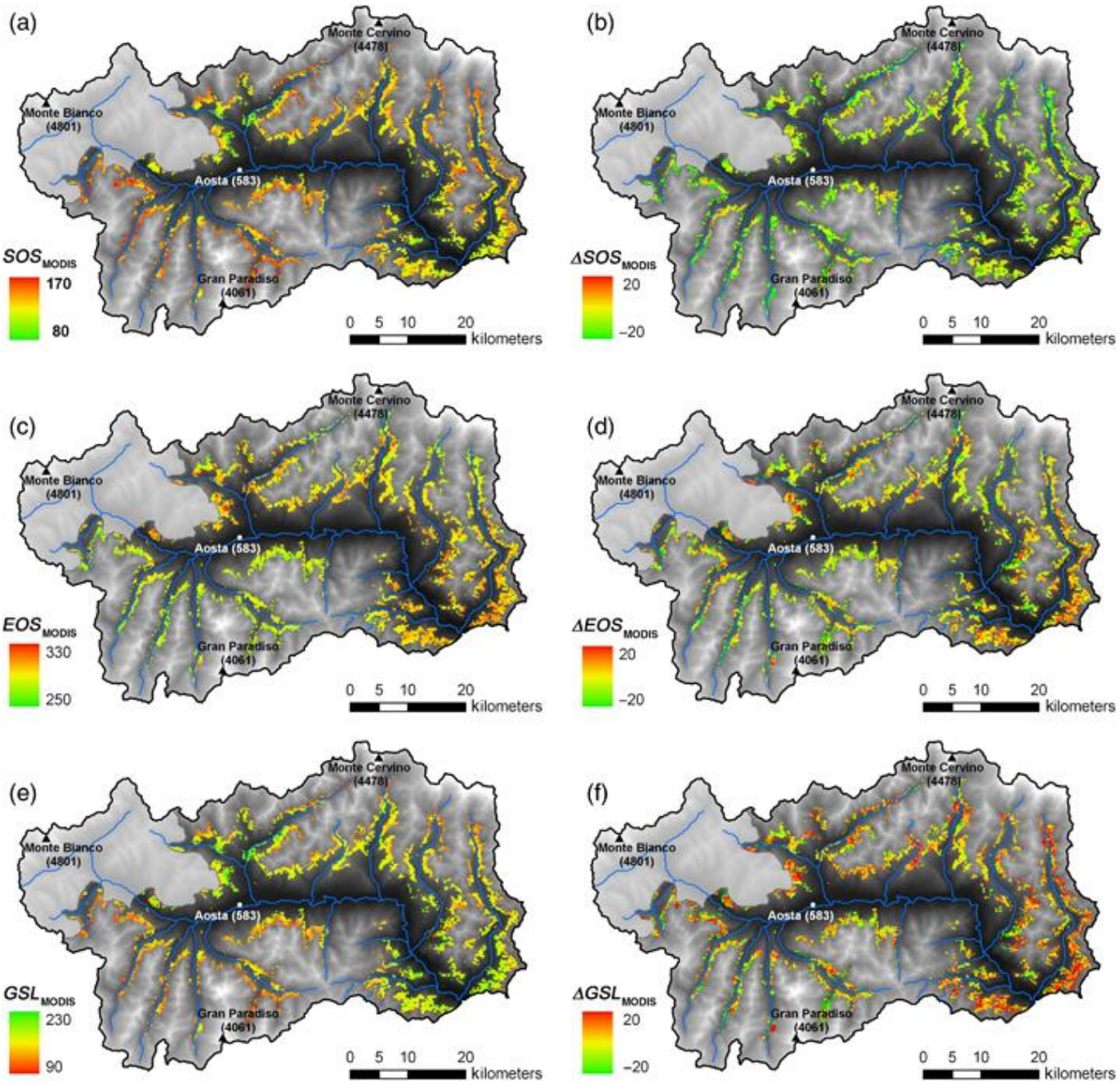

Figure 5. MODIS-derived regional maps of start and end of season and of growing season length (SOS_{MODIS}, EOS_{MODIS}, GSL_{MODIS}) (a, c, e) and of their anomalies with respect to the 2000–2007 mean (ΔSOS_{MODIS}, ΔEOS_{MODIS} and ΔGSL_{MODIS}) (b, d, f) for year 2003.

The regional means and standard deviations of SOS_{MODIS}, EDS_{MODIS} and of the corresponding anomalies in the 8 years analyzed are shown in Fig. 6.

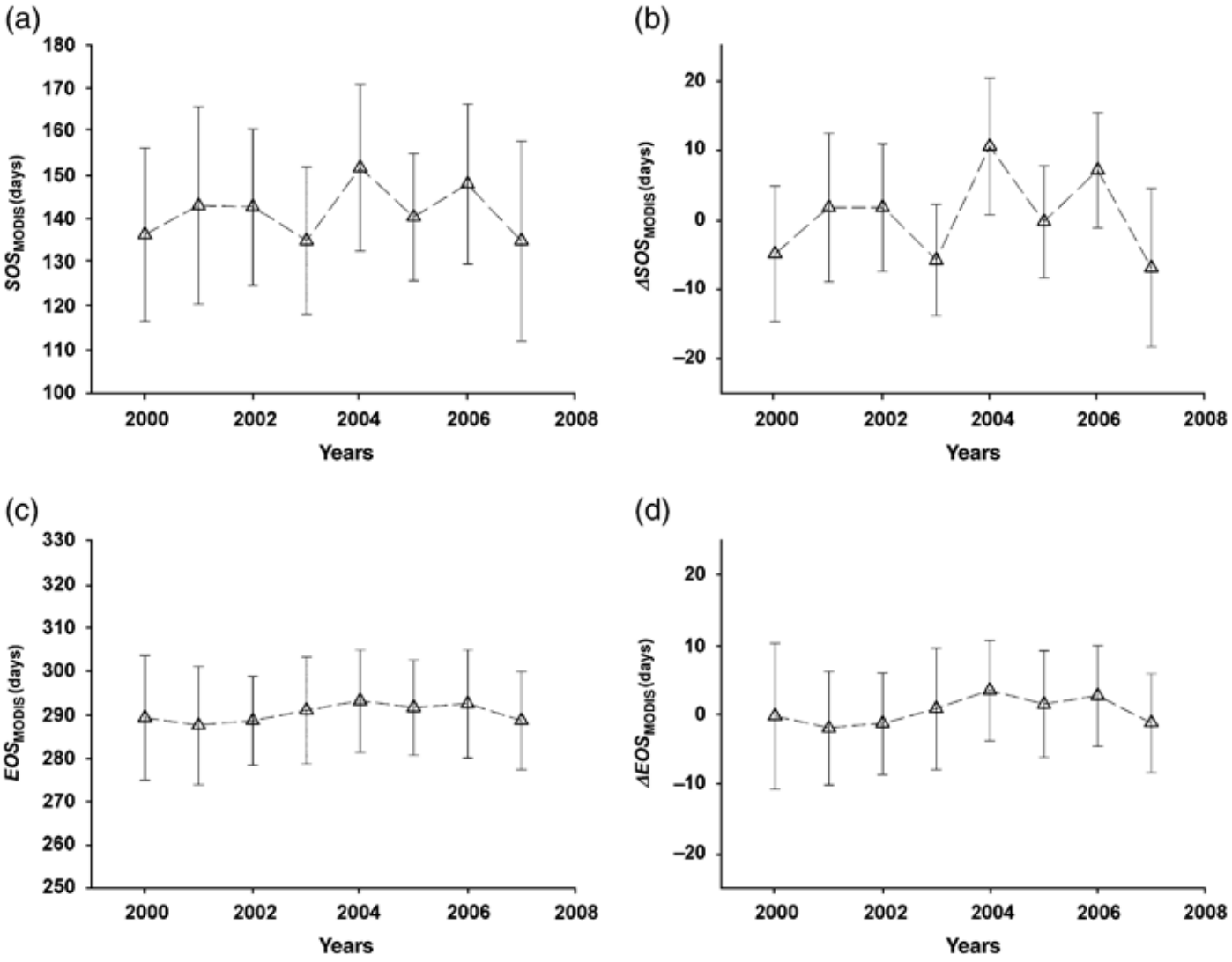

Figure 6. Mean regional values (± 1SD) of the larch start and end of season dates computed from MODIS data in 2000–2007 (SOS_{MODIS}, EOS_{MODIS}) (a, c) and of their anomalies with respect to the 2000–2007 mean (ΔSOS_{MODIS}, ΔEOS_{MODIS}) (b, d).

The interannual variations of $\overline{\Delta SOS}_{MODIS}$ highlight the strong variability of the larch start of season in the time period analyzed, showing an advance of the start of season of about 5 days in 2000, 2003 and 2007, and a delay of more than a week in 2004 and 2006. The interannual variations of $\overline{\Delta EOS}_{MODIS}$ were instead weaker, with maximum anomalies of about 2 days. This suggests that the interannual variations of the larch GSL are mostly due to variations in start of season dates, as already found in previous studies conducted on several tree species (Worrall, 1993; Walkovszky, 1998; Menzel, 2003; Menzel *et al.*, 2006).

Relationships between phenological and climate anomalies

Results of the stepwise multiple linear regression analysis between $\overline{\Delta T}_m$ and the yearly anomalies of SOS_{MODIS} and EOS_{MODIS} are shown in Table 3.

Table 3. Results of the stepwise multiple regression analysis between regional yearly anomalies of air temperature $(\overline{\Delta T}_m)$ and regional yearly anomalies of MODIS start and end of season ($\overline{\Delta SOS}_{MODIS}$, $\overline{\Delta EOS}_{MODIS}$)

Dependent variable	Predictors	R^2_{adj}	SE of the estimate	*P*	Regression model

- *P* is the statistical significance of the regression.
- *

  Anomaly of mean March, April and May air temperature.

- †

  †Anomaly of mean September air temperature.

- ‡

  ‡Anomaly of mean March, April, May and June air temperature.

$\overline{\Delta SOS}_{MODIS}$	$\overline{\Delta T}_{345}$*	0.91	2.01	<0.01 $\overline{\Delta SOS}_{MODIS} = -7.30\overline{\Delta T}_{345} + 0.29$
$\overline{\Delta EOS}_{MODIS}$	$\overline{\Delta T}_{9}$†, $\overline{\Delta T}_{2345}$‡	0.90	0.61	<0.01 $\overline{\Delta EOS}_{MODIS} = 0.99\overline{\Delta T}_{9} - 0.93\overline{\Delta T}_{2345} + 0.42$

$\overline{\Delta SOS}_{MODIS}$ was found to be strongly related to the anomalies of mean March, April and May air temperatures ($R^2_{adj} = 0.91$). The regression equation indicates that the mean start of season of larch in the Aosta valley advances (or delays) by about 7 days for each degree of increase (or decrease) in air temperature in the late winter-spring period (Fig. 7). The inclusion of other independent variables in the regression model did not yield statistically significant improvements in the explained variance.

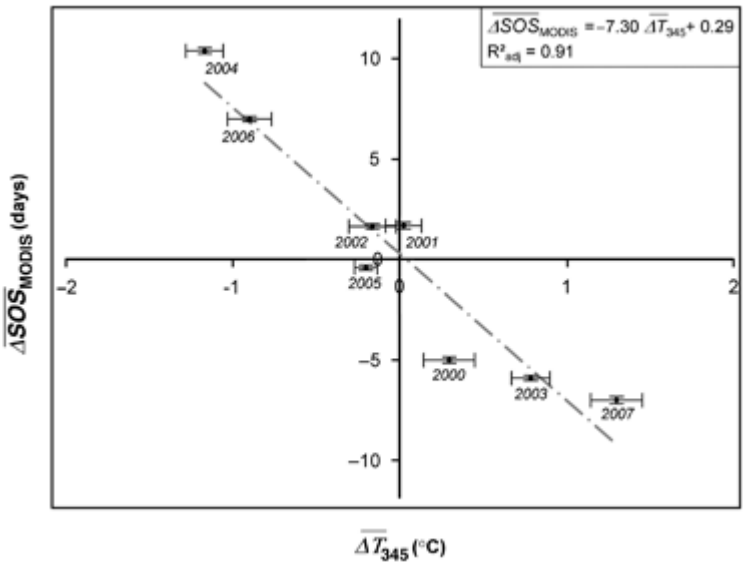

Figure 7. Regression model relating mean yearly regional anomalies of MODIS start of season ($\overline{\Delta SOS}_{MODIS}$) and mean yearly regional anomalies of March, April and May air temperature $(\overline{\Delta T}_{345})$. Error bars represent standard errors of the means.

$\overline{\Delta EOS}_{MODIS}$ was instead found to be best related to variations in mean September temperature ($R^2_{adj} = 0.77$), showing an increase in the mean end of season date of about 1 day per 1 °C increase in temperature. However, the inclusion of the February–May mean temperature anomaly as an

additional predictor in the regression model led to a statistically significant increase of R^2_{adj} of 0.13. This second predictor variable shows a negative partial correlation coefficient, suggesting that higher spring temperatures may advance the onset of leaf coloring.

Discussion

Monitoring the larch phenological cycle from MODIS data

The comparison with field observations showed that MODIS 250 m–16 days data can be successfully used to monitor the phenological cycle of European larch.

The start and end of season of larch correspond with good accuracy to NDVI metrics S_2 and A_4, and this is particularly relevant since these metrics have never been used in previous studies. The accuracy of our start of season estimates (MAE=6.39, ME=0.97) is comparable with that obtained in recent remote sensing studies. For example, Beck *et al.* (2007) found a RMSE of about 12 days (n=108, r=0.70) between observed start of season (50% of leaf buds open) of birch forests in Fennoscandia and dates estimated from MODIS 16 days data using metric S_1. Soudani *et al.* (2008) found a MAE of about 3.5 days (n=102, ME=2.0, r=0.53) between observed start of season in deciduous forests (90% of the trees with open buds over at least 20% of the crown) and metric S_3 derived from MODIS daily NDVI. Delbart *et al.* (2006) compared the observed dates of leaf appearance of birch and larch in northern Eurasia with satellite estimates obtained applying a threshold method on both NOAA-AVHRR (MAE=6.25, n=81, r=0.56, ME=0.34) and SPOT-VGT data (MAE=5.5, n=21, r=0.69, ME=0.55).

The accuracy obtained in estimating the larch end of season in this study (MAE=4.2, ME=2.3) is higher than that obtained in other remote sensing studies. For example, Karlsen *et al.* (2006) mapped the date corresponding to the shedding of 50% of birch leaves in Fennoscandia applying a threshold-based method on AVHRR data, with accuracies highly variable in the different sites analyzed (r between −0.22 and 0.97; ME variable between −1 and 26 days), while Beck *et al.* (2007) mapped the end of leaf fall of different tree species using MODIS NDVI with an estimated RMSE of about 8 days (n=25, r=0.66, ME not reported). As regards the other phenophases, the large difference observed between field-observed start of season and the half peak of the NDVI curve (metric S_3) indicates that, although this metric may be useful for analyzing relative interannual variations of the phenological cycle, its use for direct start of season estimations could lead to large overestimation errors. This is in accordance with the results of Fisher & Mustard (2007), which showed that for an oak and maple forest MODIS NDVI reached its half peak about halfway between leaf bud-burst and the date at which half of the leaves had reached 75% of their final size.

The initial decrease of the NDVI signal in the autumn season does not appear to be related to observable larch senescence processes. This may be due to the fact that the initial reduction of NDVI in our study area is probably caused by the yellowing of herbaceous understory vegetation, which generally precedes larch senescence. This may introduce uncertainties for the satellite monitoring of autumn phenophases in larch forests characterized by low fractional cover, where the variability of the satellite signal in the senescence phase is not dependant only on the coloring of larch needles. The effect of the understory on the satellite signal is instead less compelling in the spring season, since the understory begins its activity after larch bud-burst. The good accuracy of the end of season estimations obtained with metric A_4 suggests however that, even in the presence of a disturbing understory interference, MODIS data allows to accurately monitor also the main autumn phenological phases of larch.

Satellite vs. phenological models estimates

Results of this study indicate that the overall accuracy of phenological models in estimating the start and end of season dates of larch is lower than that obtained from MODIS data.

Although the SW model outperformed MODIS in predicting the start of season in most of the sites, the strong underestimation observed at the Etroubles site in 2007 poses serious doubts about its suitability for larch phenology monitoring. The observed underestimation has probably two explanations. Firstly, data from this site were not used for model optimization due to unavailability of field data in year 2005 (Migliavacca *et al.*, 2008). Since Etroubles is the monitoring site characterized by the lowest elevation (1350 m) and is an artificial plantation located almost outside the larch natural distribution elevation range, this may lead to application of the model outside of its proper validity range (defined by the characteristics of the sites used for optimization in terms of elevation, climate, etc.). The same consideration may also explain the strong error observed in the end of season estimates obtained with GSI at the Etroubles site. The SW underestimation may be also due to the considerably warmer late winter and early spring temperatures observed in 2007 with respect to 2005 and 2006 (e.g., January mean temperature 6 °C higher in 2007). At low altitude sites, the SW baseline temperature was therefore exceeded even in the middle of winter, leading to a very early start of season estimation.

On the basis of these observations, it can be argued that phenological models driven by air temperature only are unable to describe the processes governing larch phenology in anomalous climatic conditions. This consideration is also supported by the accuracy of the 2007 SOS_{GSI} estimate at the Etroubles site, which is similar to that of the other sites. Even if high air temperatures are recorded in winter and early spring SOS_{GSI} is not anticipated as much as it occurs to SOS_{SW}, because GSI also accounts for photoperiod limitations in plant development. Although several studies suggest that photoperiod is not generally involved in spring development (e.g., Hunter & Lechowicz, 1992), in anomalous warm years it may act as a limiting factor which inhibits or postpones the exit from the dormant phase, and guarantees that the larch does not start its growing cycle too early, when extremely low temperatures may still occur (Linkosalo, 2000; Stöckli *et al.*, 2008).

These considerations have important implications for phenological monitoring at continental or global scale. Climate-driven phenological models need to be parameterized against local field observations and assume that the response of the analyzed species or vegetation type to climate variations is spatially constant. If this assumption does not hold, the accuracy of phenological dates estimated by these models can be expected to be spatially variable to a large extent, reflecting the variability in climate–phenology relationships (e.g., Richardson *et al.*, 2006; Fisher *et al.*, 2007). On the contrary, the accuracy of satellite estimates should be more spatially homogeneous. Remote sensing methods are in fact based on the direct observation of phenological events, and they do not require an *a priori* parameterization based on local observations. Moreover, these methods do not require the availability of accurate maps of the phenology drivers (e.g., air temperature, vapor pressure deficit), which are instead used by climate-driven models. This is particularly important for phenological monitoring in morphologically complex areas like the Alps, where the realization of meteorological maps with sufficient spatial resolution is very difficult. Besides the afore-mentioned advantages, remote sensing methods lack the predictive power of phenological models, and cannot therefore be used to estimate the effects that the expected future climatic variations will exert on terrestrial ecosystems.

Response of larch phenology to climate variability

The strong response of MODIS-derived start of season at regional level to spring temperature variations highlights the great influence of climate on this phenological variable. The magnitude of the response identified in this study is in accordance with results of previous studies based instead on analysis of field data. For example, Chmielewski & Rötzer (2001) reported that bud-burst of different deciduous European tree species advances on the average of 7 days for a 1 °C increase in mean February-April temperatures. Walkovszky (1998) also reported that a 1 °C rise of mean early spring temperature causes a 7-day advanced flowering of *Robinia pseudoacacia*. Menzel (2003) found advances in leaf unfolding of different tree species in Germany between 2.5 and 4.7 days per 1 °C increase in spring temperatures.

As regards the end of season, positive anomalies of autumn temperatures were found to lead only to slight delays in the onset of leaf coloring. This is probably a consequence of the fact that leaf coloring is also strongly influenced by photoperiod, which in Alpine regions in autumn generally becomes limiting before air temperature (Migliavacca *et al.*, 2008; Stöckli *et al.*, 2008). Our results also suggest that a relatively earlier onset of needle coloring is observed after warm springs and summers. In years characterized by high spring temperatures, the lengthening of the growing season caused by the earlier start of season may be therefore partially contrasted by a concurring advance of the end of season. This confirms the results of other studies conducted both on larch (Worrall, 1993) and other forest species (Menzel, 2003) and, according to Worrall (1993), it may be due to the acceleration of leaf aging processes caused by high temperatures. Considering the short time span of the available data set, additional research should however be undertaken to verify the significance of the effect of spring temperatures on larch senescence.

Conclusions

In this study, we investigated the relationships between the field-observed dynamics of the European larch phenological cycle and MODIS NDVI time series, and quantitatively assessed the response of the larch phenological cycle to climate variability in Alpine regions.

Results showed that MODIS 250 m data can be effectively used for phenological monitoring in Alpine forests, where field phenological monitoring is seldom performed. In particular, the start and end of the larch growing season can be estimated with good accuracy from the computation of the roots of the third derivative of logistic curves fitted to MODIS NDVI time series. We believe that the achieved accuracy can allow the use of satellite data for analyzing the spatial and interannual variability of larch phenology in rugged mountainous terrain.

Comparison with field observations also suggested that the estimation of spatial and interannual variations of the main phenological dates of larch achieved by satellite monitoring is more accurate than that obtained by climate-driven phenological models, which may suffer from the assumption of spatially invariant climate/phenology relationships and from an incomplete description of the processes. Finally, the interannual variability of phenology as seen from MODIS data was found to be closely linked to regional climatic variability. This demonstrates that a combined analysis of satellite images and local meteorological measurements may allow quantifying the response of the phenological cycle of forest ecosystems to climatic variability in Alpine regions.

Acknowledgements

This research was conducted in the framework of the REPHLEX (Remote Sensing of larch Phenology Experiment) Project, funded by the Environmental Protection Agency of Aosta Valley. The authors thank L. Ganis (ARPA VDA) for his support in field data collection. We also thank the anonymous reviewers and the editors for their helpful comments during the revision of this manuscript.

References

Ahl DE, Gower ST, Burrows SN, Shabanov NV, Myneni RB, Knyazikhin Y (2006) Monitoring spring canopy phenology of a deciduous broadleaf forest using MODIS. Remote Sensing of Environment, 104, 88–95.

Badeck FW, Bondeau A, Bottcher K, Doktor D, Lucht W, Schaber J, Sitch S (2004) Responses of spring phenology to climate change. New Phytologist, 162, 295–309.

Beck PSA, Atzberger C, Hogda KA, Johansen B, Skidmore AK (2006) Improved monitoring of vegetation dynamics at very high latitudes: a new method using MODIS NDVI. Remote Sensing of Environment, 100, 321–334.

Beck PSA, Jonsson P, Hogda KA, Karlsen SR, Eklundh L, Skidmore AK (2007) A ground-validated NDVI dataset for monitoring vegetation dynamics and mapping phenology in Fennoscandia and the Kola peninsula. International Journal of Remote Sensing, 28, 4311–4330.

Beniston M, Rebetez M (1996) Regional behavior of minimum temperatures in Switzerland for the period 1979–1993. Theoretical and Applied Climatology, 53, 231–243.

Bogaert J, Zhou L, Tucker CJ, Myneni RB, Ceulemans R (2002) Evidence for a persistent and extensive greening trend in Eurasia inferred from satellite vegetation index data. Journal of Geophysical Research-Atmospheres, 107, 4119–4127.

Campbell GS, Norman JM (1998) An Introduction to Environmental Biophysics. Springer, Berlin.

Cayan DR, Kammerdiener SA, Dettinger MD, Caprio JM, Peterson DH (2001) Changes in the onset of spring in the western United States. Bulletin of the American Meteorological Society, 82, 399–415.

Chen J, Jonsson P, Tamura M, Gu ZH, Matsushita B, Eklundh L (2004) A simple method for reconstructing a high-quality NDVI time-series data set based on the Savitzky–Golay filter. Remote Sensing of Environment, 91, 332–344.

Chen XQ, Tan ZJ, Schwartz MD, Xu CX (2000) Determining the growing season of land vegetation on the basis of plant phenology and satellite data in Northern China. International Journal of Biometeorology, 44, 97–101.

Chmielewski FM, Rötzer T (2001) Response of tree phenology to climate change across Europe. Agricultural and Forest Meteorology, 108, 101–112.

Chmielewski FM, Rötzer T (2002) Annual and spatial variability of the beginning of growing season in Europe in relation to air temperature changes. Climate Research, 19, 257–264.

Chuine I (2000) A unified model for budburst of trees. Journal of Theoretical Biology, 207, 337–347.

Colombo R, Busetto L, Migliavacca M et al. (2009) On the spatial and temporal variability of Larch phenological cycle in mountainous areas. Italian Journal of Remote Sensing, 41, 79–96.

Cook BI, Smith TM, Mann ME (2005) The North Atlantic Oscillation and regional phenology prediction over Europe. Global Change Biology, 11, 919–926.

Defila C, Clot B (2001) Phytophenological trends in Switzerland. International Journal of Biometeorology, 45, 203–207.

Delbart N, Kergoat L, Le Toan T, Lhermitte J, Picard G (2005) Determination of phenological dates in boreal regions using normalized difference water index. Remote Sensing of Environment, 97, 26–38.

Delbart N, Le Toan T, Kergoat L, Fedotova V (2006) Remote sensing of spring phenology in boreal regions: a free of snow-effect method using NOAA-AVHRR and SPOT-VGT data (1982–2004). Remote Sensing of Environment, 101, 52–62.

Delbart N, Picard G, Le Toans T et al. (2008) Spring phenology in boreal Eurasia over a nearly century time scale. Global Change Biology, 14, 603–614.

Delpierre N, Dufrene E, Soudani K, Ulrich E, Cecchini S, Boé J, Francois C (2009) Modelling interannual and spatial variability of leaf senescence for three deciduous tree species in France. Agricultural and Forest Meteorology, 149, 938–948.

Fisher JI, Mustard JF (2007) Cross-scalar satellite phenology from ground, Landsat, and MODIS data. Remote Sensing of Environment, 109, 261–273.

Fisher JI, Mustard JF, Vadeboncoeur MA (2006) Green leaf phenology at Landsat resolution: scaling from the field to the satellite. Remote Sensing of Environment, 100, 265–279.

Fisher JI, Richardson AD, Mustard JF (2007) Phenology model from surface meteorology does not capture satellite-based greenup estimations. Global Change Biology, 13, 707–721.

Fu P, Rich PM (1999) Design and implementation of the Solar Analyst: an ArcView extension for modeling solar radiation at landscape scales. 19th Annual ESRI User Conference. San Diego, USA.

Huete A, Didan K, Miura T, Rodriguez EP, Gao X, Ferreira LG (2002) Overview of the radiometric and biophysical performance of the MODIS vegetation indices. Remote Sensing of Environment, 83, 195–213.

Hunter AF, Lechowicz MJ (1992) Predicting the timing of budburst in temperate trees. Journal of Applied Ecology, 29, 597–604.

Janssen PHM, Heuberger PSC (1995) Calibration of process-oriented models. Ecological Modelling, 83, 55–66.

Jolly WM, Nemani R, Running SW (2005) A generalized, bioclimatic index to predict foliar phenology in response to climate. Global Change Biology, 11, 619–632.

Karlsen SR, Elvebakk A, Høgda KA, Johansen B (2006) Satellite-based mapping of the growing season and bioclimatic zones in Fennoscandia. Global Ecology and Biogeography, 15, 416–430.

Kramer K, Leinonen I, Loustau D (2000) The importance of phenology for the evaluation of impact of climate change on growth of boreal, temperate and Mediterranean forests ecosystems: an overview. International Journal of Biometeorology, 44, 67–75.

Lieth H (1974) Phenology and Seasonality Modeling. Springer, Heidelberg.

Linkosalo T (2000) Analyses of the spring phenology of boreal trees and its response to climate change. Unpublished PhD Dissertation, Department of Forest Ecology Publications 22, University of Helsinki, 55pp.

Markwardt CB (2008) Non-linear least squares fitting in IDL with MPFIT. Astronomical Data Analysis Software and Systems XVIII. Quebec, Canada.

Matsumoto K, Ohta T, Irasawa M, Nakamura T (2003) Climate change and extension of the Ginkgo biloba L. growing season in Japan. Global Change Biology, 9, 1634–1642.

Menzel A (2003) Plant phenological anomalies in Germany and their relation to air temperature and NAO. Climatic Change, 57, 243–263.

Menzel A, Fabian P (1999) Growing season extended in Europe. Nature, 397, 659.

Menzel A, Sparks TH, Estrella N et al. (2006) European phenological response to climate change matches the warming pattern. Global Change Biology, 12, 1969–1976.

Migliavacca M, Cremonese E, Colombo R et al. (2008) European larch phenology in the Alps: can we grasp the role of ecological factors by combining field observations and inverse modelling? International Journal of Biometeorology, 52, 587–605.

Myneni RB, Keeling CD, Tucker CJ, Asrar G, Nemani RR (1997) Increased plant growth in the northern high latitudes from 1981 to 1991. Nature, 386, 698–702.

Nash JE, Sutcliffe JV (1970) River flow forecasting through conceptual models part I – a discussion of principles. Journal of Hydrology, 10, 282–290.

Picard G, Quegan S, Delbart N, Lomas MR, Le Toan T, Woodward FI (2005) Bud-burst modelling in Siberia and its impact on quantifying the carbon budget. Global Change Biology, 11, 2164–2176.

Potts JT, Shi XRR, Raven PB (1993) Carotid baroreflex responsiveness during dynamic exercise in humans. American Journal of Physiology, 265, H1928–H1938.

Reed BC, Brown JF, Vanderzee D, Loveland TR, Merchant JW, Ohlen DO (1994) Measuring phenological variability from satellite imagery. Journal of Vegetation Science, 5, 703–714.

Richardson AD, Bailey AS, Denny EG, Martin CW, O'Keefe J (2006) Phenology of a northern hardwood forest canopy. Global Change Biology, 12, 1174–1188.

Rötzer T, Wittenzeller M, Haeckel H, Nekovar J (2000) Phenology in central Europe – differences and trends of spring phenophases in urban and rural areas. International Journal of Biometeorology, 44, 60–66.

Sakamoto T, Yokozawa M, Toritani H, Shibayama M, Ishitsuka N, Ohno H (2005) A crop phenology detection method using time-series MODIS data. Remote Sensing of Environment, 96, 366–374.

Schaber J, Badeck FW (2002) Evaluation of methods for the combination of phenological time series and outlier detection. Tree Physiology, 22, 973–982.

Schaber J, Badeck FW (2005) Plant phenology in Germany over the 20th century. Regional Environmental Change, 5, 37–46.

Schwartz MD, Reed BC (1999) Surface phenology and satellite sensor-derived onset of greenness: an initial comparison. International Journal of Remote Sensing, 20, 3451–3457.

Schwartz MD, Reiter BE (2000) Changes in North American spring. International Journal of Climatology, 20, 929–932.

Schwartz MD, Reed BC, White MA (2002) Assessing satellite-derived start-of-season measures in the conterminous USA. International Journal of Climatology, 22, 1793–1805.

Slayback DA, Pinzon JE, Los SO, Tucker CJ (2003) Northern hemisphere photosynthetic trends 1982–99. Global Change Biology, 9, 1–15.

Soudani K, Le Maire G, Dufrene E, Francois C, Delpierre N, Ulrich E, Cecchini S (2008) Evaluation of the onset of green-up in temperate deciduous broadleaf forests derived from Moderate Resolution Imaging Spectroradiometer (MODIS) data. Remote Sensing of Environment, 112, 2643–2655.

Stöckli R, Vidale PL (2004) European plant phenology and climate as seen in a 20-year AVHRR land-surface parameter dataset. International Journal of Remote Sensing, 25, 3303–3330.

Stöckli R, Rutishauser T, Dragoni D et al. (2008) Remote sensing data assimilation for a prognostic phenology model. Journal of Geophysical Research-Biogeosciences, 113, 19.

Studer S, Appenzeller C, Defila C (2005) Inter-annual variability and decadal trends in alpine spring phenology: a multivariate analysis approach. Climatic Change, 73, 395–414.

Studer S, Stöckli R, Appenzeller C, Vidale PL (2007) A comparative study of satellite and ground-based phenology. International Journal of Biometeorology, 51, 405–414.

Theurillat J-P, Guisan A (2001) Potential impact of climate change on vegetation in the European Alps: a review. Climatic Change, 50, 77–109.

Walkovszky A (1998) Changes in phenology of the locust tree (Robinia pseudoacacia L) in Hungary. International Journal of Biometeorology, 41, 155–160.

White MA, Brunsell NA, Schwartz MD (2003) Vegetation phenology in global change studies. In: Phenology: An Integrative Environmental Science (ed. SchwartzMD), 453–466. Kluwer, Dordrecht.

White MA, De Beurs KM, Didan K et al. (2009) Intercomparison, interpretation, and assessment of spring phenology in North America estimated from remote sensing for 1982–2006. Global Change Biology, 10, 2335–2359.

White MA, Thornton PE, Running SW (1997) A continental phenology model for monitoring vegetation responses to interannual climatic variability. Global Biogeochemical Cycles, 11, 217–234.

Worrall J (1993) Temperature effects on bud-burst and leaf-fall in subalpine larch. Journal of Sustainable Forestry, 1, 1–18.

Worrall J (1999) Phenology and the changing seasons. Nature, 399, 101.

Zhang XY, Friedl MA, Schaaf CB et al. (2003) Monitoring vegetation phenology using MODIS. Remote Sensing of Environment, 84, 471–475.

Zhou LM, Tucker CJ, Kaufmann RK, Slayback D, Shabanov NV, Myneni RB (2001) Variations in northern vegetation activity inferred from satellite data of vegetation index during 1981 to 1999. Journal of Geophysical Research-Atmospheres, 106, 20069–20083.